Weak-inertial flow between two rough surfaces

David Lo Jacono, Franck Plouraboué, Alain Bergeon

Weak-inertial flow between two rough surfaces

D. Lo Jacono[a)]
Laboratory of Fluid Mechanics, Swiss Federal Institute of Technology Lausanne, Ecole Polytechnique Federal Lausanne (EPFL), CH-1015 Lausanne, Switzerland

F. Plouraboué and A. Bergeon
Institut de Mécanique des Fluides de Toulouse, Unité Mixte de Recherche, Centre National de la Recherche Scientifique (CNRS) 5502, Université Paul Sabatier, UFR MIG 118, route de Narbonne, 31062 Toulouse, France

(Received 3 June 2004; accepted 28 March 2005; published online 26 May 2005)

"Oseen–Poiseuille" equations are developed from an asymptotic formulation of the three-dimensional Navier–Stokes equations in order to study the influence of weak inertia on flows between rough surfaces. The impact of the first correction on macroscopic flow due to inertia has been determined by solving these equations numerically. From the numerical convergence of the asymptotic expansion to the three-dimensional Navier–Stokes flows, it is shown that, at the macroscopic scale, the quadratic correction to the Reynolds equation in the weak-inertial regime vanishes generalizing a similar result in porous media. © *2005 American Institute of Physics*.
[DOI: 10.1063/1.1923347]

I. INTRODUCTION

The study of weak-inertial effects between two rough surfaces is of interest in several contexts. It has been, for example, investigated in microfluidic applications where the Reynolds numbers are generally small while the flow is laminar and sometimes inefficient for mixing purpose. In those cases, weak-inertial effects as those studied by Sobey[1] and Jones, Thomas, and Aref[2] could lead to important consequences on stirring. Approximating inertial effects with asymptotic analysis is interesting for it avoids solving heavy three-dimensional Navier–Stokes equations in complicated geometries. For example, in cylindrical geometries, the Dean[3,4] approximation for curved pipes has been used to study inertially driven chaotic advection.[2] Recent experimental results[5] have shown that proper surface patterning could generate vortex which are transverse to the longitudinal mean flow that could be used to produce chaotic stirring.[6] These experiments have been successfully analyzed in the context of Stokes flows, in the limit of small patterning amplitude.[7] Small amplitude perturbation has also been discussed to investigate inertial effects in two-dimensional corrugated surfaces.[8,9] In this paper we discuss another interesting limit associated with smooth boundary variations, or similarly, three-dimensional channels having large aspect ratio. The procedure is similar to the long-wavelength expansion used in the study of falling films in two[10–14] or three dimensions.[15,16] Contrary to the problem of fluid flows confined between rigid surfaces, that of falling films is a free-boundary problem which generally involves different nondimensional numbers such as the Bond number, capillary number, and Reynolds number. Depending on the capillary number, the influence of inertia could be obtained either in a closed form by ignoring surface-tension effects, or within an implicit perturbation expansion for a finite capillary number.[13] Numerical calculations have nevertheless shown that for any capillary number in two dimensions the generalization of lubrication theory, including first inertial perturbations, extends by more than one order of magnitude the range of applicability of standard lubrication theory.[13] This observation has led to the present study to assess the validity range of inertial effects described through a generalization of lubrication theory in the context of confined flow between complicated corrugated surfaces. In this context Sawyers, Sen, and Chang[17] proposed such a long-wavelength expansion for the Navier–Stokes equations associated with a three-dimensional anisotropic (one longitudinal direction variations are supposed much larger than the transverse one) sinusoidal walls. Siddique and Khayat[18] have also studied numerically geometrically forced inertial effects in three-dimensional cavities presenting two-dimensional spatial variations.

In this paper we derive the first inertial correction to lubrication theory for flow in between three-dimensional general surfaces, having similar variations in the horizontal plane. We discuss this approximation for various boundary conditions over a wide range of Reynolds number.

Another related issue discussed in the porous media literature is the macroscopic impact of the Navier inertial term on the usual macroscopic relation between the mean pressure and the mean flux. Using homogenization theory, Mei and Auriault[19] derived general relationships between pressure and velocity at macroscopic scale for an isotropic homogeneous porous media. They obtained a cubic correction for the macroscopic pressure gradient as a function of the macroscopic imposed flux. Further experimental measurements and numerical simulations have shown that the range of validity of this cubic regime is quite narrow and confined to small Reynolds numbers.[20] For larger Reynolds numbers, one recovers the Darcy–Forcheimer quadratic correction to the

[a)]Author to whom correspondence should be addressed. Electronic mail: david.lojacono@epfl.ch

macroscopic pressure gradient. More recently, Skejtne, Hansen, and Gudmundsson[21] have performed numerical simulations of high velocity flows in fractures made of self-affine two-dimensional walls using full Navier–Stokes equations. Of interest for this work is the cubic correction observed numerically by the authors in the weak-inertial regime. To our knowledge, no theoretical analysis of inertial effects has been developed for flows through fractures. Understanding these effects cannot be achieved in the light of results available for flows in heterogeneous porous media. Because the lubrication approximation leads to a local Darcy relation, flows through fractures can be regarded as two-dimensional flows across a specific porous media. However, this analogy cannot be extended to include inertial effects generalizing the results of Mei and Auriault[19] to flows in fractures. The analysis of macroscopic inertial effects on fracture flows first requires a generalization of lubrication theory including inertia.

Hence, Sec. II A presents the asymptotic expansion of the lubrication theory leading to the two-dimensional Oseen–Poiseuille equations. Those equations are solved analytically in the limit of small amplitude in Sec. II B. Section III is concerned with the numerical solution and the validity of the asymptotic Oseen–Poiseuille equations, as previously investigated by Sawyers, Sen, and Chang[17] for anisotropic three-dimensional surfaces. The Oseen–Poiseuille equations are solved numerically with a method described in Sec. III A and validated in Sec. III B. Section III B 2 discusses the physics of inertial effect in a simple example for which the aperture perturbation displays a simple sinusoidal shape. The two-dimensional numerical solutions are then compared with the numerical solutions of the full three-dimensional Navier–Stokes equations in Sec. III B 3. In Sec. IV the macroscopic effect of the first inertial corrections on the Oseen–Poiseuille equations is investigated using two complementary macroscopization techniques. It is demonstrated that quadratic corrections in the weak-inertial regime vanish in favor of nonzero cubic inertial corrections. Those cubic corrections are recovered by means of three-dimensional computations of the Navier–Stokes equations.

II. OSEEN–POISEUILLE WEAK-INERTIAL EQUATIONS

A. Governing equation and inertial correction

In this section, the equations for first-order inertial correction to the lubrication approximation are established. The fracture is described by the volume inbetween two rough surfaces $Z_1(X,Y)$ and $Z_2(X,Y)$ where (X,Y,Z) are the Cartesian coordinates. We define L as the horizontal extension in the X and Y directions and $H(X,Y)=Z_2-Z_1>0$ as the aperture. We focus on a flow through a thin and smooth fracture where the local slope of each surfaces ϵ is small $\epsilon \ll 1$. Moreover, the mean aperture $\langle H\rangle = \int_0^L\int_0^L H(X,Y)dXdY/L^2$ is small compared to the typical horizontal extension L of the fracture. We study situations in which viscosity and inertial effects are of the same order of magnitude and the boundary layer fills all of the gap between the two rough surfaces. The condition for the boundary layer to be fully developed on the typical length $\langle H\rangle/\epsilon$ gives a condition related to the Reynolds number $\nu\langle H\rangle/\langle U\rangle\epsilon \geqslant \langle H\rangle^2$ or equivalently, $\mathrm{Re}\,\epsilon \leqslant 1$, where $\mathrm{Re}=\langle U\rangle\langle H\rangle/\nu$ is the Reynolds number based on the characteristic velocity $\langle U\rangle$ and the kinematic viscosity ν. This condition is also used by Tuck and Kousoubov[22] for investigating the influence of entry effects due to inertial on boundary conditions. We will consider that the boundary layers associated with the upper and lower surfaces are fully developed from upstream conditions so that no restriction on the upper Reynolds number values will be explicitly considered in the following as far as boundary layers are concerned. We will nevertheless consider "moderate" inertial effects, the precise meaning of which will later be discussed. On the contrary, beside $O(\epsilon^2)$ Stokes corrections to lubrication theory are not considered in the following; it turns out that lubricated inertial effects of the order $\mathrm{Re}\,\epsilon$ should self-consistently be larger. Hence the range of the Reynolds number concerned by the following analysis is $c/\epsilon > \mathrm{Re} \gg \epsilon$, where c is a constant whose value will be discussed in the light of the numerical results of Sec. III B 3. Finally, we wish to illustrate the relevance of moderate inertial effects on a simple example. Let us evaluate the Reynolds number associated with water flowing through a channel whose vertical gap is one-tenth of millimeter with a velocity of 1 cm/s. Given the kinematic viscosity of water ($\nu=10^{-6}$ m^2/s), one easily finds that $\mathrm{Re}=1$ in that case. Hence, moderate velocities associated with submillimeter dimensions and usual fluids could lead to moderate inertial effects which we have studied here. Similar conclusions have been reached in the context of falling films.[11,13]

The fields are then nondimensionalized using $\langle H\rangle/\epsilon$ and $\langle H\rangle$ for distances in the horizontal and vertical directions, respectively, the averaged horizontal velocity $\langle U\rangle$ for the velocity, and the usual viscous lubrication pressure $\mu\langle U\rangle/\epsilon\langle H\rangle$ for the pressure, where μ is the fluid dynamic viscosity. Using this scaling, and keeping the same notation for dimensionless variables, the incompressibility condition for the velocity field reads

$$\tilde{\nabla}\cdot\mathbf{U}=0 \quad \text{with } \tilde{\nabla}\equiv\left(\partial_X,\partial_Y,\frac{1}{\epsilon}\partial_Z\right), \tag{1}$$

leading to the following self-consistent **nondimensional** velocity scaling, $\mathbf{U}=(u,v,\epsilon w)$. The dimensionless Navier–Stokes equations are

$$\begin{aligned}
&\mathrm{Re}\,\epsilon\,(u\partial_X u+v\partial_Y u+w\partial_Z u)=-\partial_X p+\partial_Z^2 u,\\
&\mathrm{Re}\,\epsilon\,(u\partial_X v+v\partial_Y v+w\partial_Z v)=-\partial_Y p+\partial_Z^2 v,\\
&\mathrm{Re}\,\epsilon^3\,(u\partial_X w+v\partial_Y w+w\partial_Z w)=-\partial_Z p+\epsilon^2\partial_Z^2 w.
\end{aligned} \tag{2}$$

We next expand the pressure and velocity fields in powers of ϵ,

$$(p,\mathbf{U},\mathbf{q})=(p_0,\mathbf{U}_0,\mathbf{q}_0)+\mathrm{Re}\,\epsilon(p_1,\mathbf{U}_1,\mathbf{q}_1)+O(\epsilon^2,\mathrm{Re}^2\,\epsilon^2), \tag{3}$$

where the subscripts refer to the order of the correction and where $\mathbf{q}$ is the horizontal flux obtained after integration of the velocity across the local aperture $\mathbf{q}=\int_{Z_1}^{Z_2}(u,v)dz$. The

leading order gives the classical lubrication boundary layer equations:

$$\begin{aligned} \mathbf{0} &= -\,\boldsymbol{\nabla} p_0 + \partial_Z^2 \mathbf{u}_0, \\ 0 &= -\,\partial_Z p_0, \end{aligned} \tag{4}$$

where $\boldsymbol{\nabla} \equiv (\partial_X, \partial_Y)$ and $\mathbf{u}_0 \equiv (u_0, v_0)$ are the two-dimensional leading-order velocity fields. These equations are easily solved using no-slip boundary conditions $\mathbf{u}_0 = \mathbf{0}$ along $Z = Z_1$ and $Z = Z_2$. One recovers the usual Reynolds equations with a Poiseuille profile of the in-plane velocity field $\mathbf{u}_0 = (1/2)(Z - Z_1)(Z - Z_2)\boldsymbol{\nabla} p_0$. Integrating this profile in the vertical direction gives the Darcy–Reynolds relation between the flux $\mathbf{q}_0$ and the pressure field, $\mathbf{q}_0 = -(2Z_-^3/3)\boldsymbol{\nabla} p_0 = -(H^3/12)\boldsymbol{\nabla} p_0$, where $Z_- = (Z_2 - Z_1)/2 = H/2$. The flux $\mathbf{q}_0$ is divergence free and the pressure $p_0 \equiv p_0(X, Y)$ satisfies

$$\boldsymbol{\nabla} \cdot (H^3 \boldsymbol{\nabla} p_0) = 0. \tag{5}$$

One can obtain the vertical velocity component w_0, from the divergence-free condition (1). Since w_0 is a third-order polynomial in Z, it cannot fulfill the no-slip boundary conditions along the surfaces $Z = Z_1$ and $Z = Z_2$. This apparent inconsistency disappears when one realizes that lubrication approximation should be written on the relative curvilinear mean reference surface defined by $Z_+(x,y) = [Z_1(x,y) + Z_2(x,y)]/2$. Let us define by (x,y,z) the curvilinear coordinate system in which (x,y) are the orthogonal curvilinear coordinates lying on the surface $Z = Z_+$ and z is parallel to the vertical coordinate with $z = Z - Z_+(x,y)$. Therefore, (x,y,z) defines a nonorthogonal curvilinear coordinate system in which the (x,y) part of the metric tensor is diagonal. In this coordinate system, Euclidean differential operators must be translated into covariant derivative operators. But a striking simplification can be obtained because the deviations of these covariant differential operators from their Euclidean form are small when the mean reference surface deviations from a plane are small. More precisely, if the typical slopes of these variations are $O(\epsilon)$, the covariant derivatives $(\mathcal{D}_x, \mathcal{D}_y)$ differ from the Euclidean version (∂_X, ∂_Y) by $O(\epsilon^2)$.[23] Hence, regarding the order of the expansion (3), the covariant derivatives in the curvilinear coordinates (x,y,z) will be self-consistently identified hereafter with their corresponding Cartesian (X,Y,Z) formulation. One can easily recover the expression for the leading-order velocity field in the curvilinear coordinates (x,y,z). Integration of Eq. (4) with the no-slip boundary conditions $\mathbf{u}_0(x,y,z = \pm Z_-) = \mathbf{0}$ leads to the parabolic velocity profile $\mathbf{u}_0 = 1/2\boldsymbol{\nabla} p_0(z^2 - Z_-^2)$ and Eq. (1) gives

$$\partial_z w_0 = -\,\boldsymbol{\nabla} \cdot \mathbf{u}_0, \tag{6}$$

where $\boldsymbol{\nabla} \equiv (\partial_x, \partial_y) = (\partial_X, \partial_Y) + O(\epsilon^2)$. Integrating (6) with the symmetric boundary conditions $w_0(x,y,z = \pm Z_-) = 0$ and simplifying this result using (5) lead to

$$w_0 = -\frac{\Delta p_0}{6} z(z^2 - Z_-^2), \tag{7}$$

which displays the correct antisymmetric vertical profile in the relative coordinates (x,y,z). The next Oseen term accounting for inertial effects is obtained after substitution of expansion (3) in (2), leading to

$$\begin{aligned} \mathbf{u}_0 \cdot \boldsymbol{\nabla} \mathbf{u}_0 + w_0 \partial_z \mathbf{u}_0 &= -\,\boldsymbol{\nabla} p_1 + \partial_z^2 \mathbf{u}_1, \\ 0 &= \partial_z p_1. \end{aligned} \tag{8}$$

This correction to the leading-order lubrication flow still displays a boundary layer structure, with a pressure correction p_1 being uniform in the vertical direction. The correction $\mathbf{u}_1$ can be obtained analytically from Eq. (8) using the no-slip boundary conditions $\mathbf{u}_1(x,y,z = \pm Z_-) = 0$ and reads

$$\mathbf{u}_1 = (z^2 - Z_-^2)\left\{ \frac{\boldsymbol{\nabla} p_1}{2} + (z^4 - 4z^2 Z_-^2 + 11 Z_-^4)\left[\frac{\boldsymbol{\nabla}(\boldsymbol{\nabla} p_0)^2}{240} + \frac{\boldsymbol{\nabla} p_0 (\boldsymbol{\nabla} p_0 \cdot \boldsymbol{\nabla} Z_-)}{60 Z_-} \right] \right\}. \tag{9}$$

From the in-plane inertial correction (9), one can obtain the related flux after integration in the vertical direction. This leads to the same inertial pressure/flux dependence as the lubrication leading order, plus some nontrivial inertial terms depending on the leading-order pressure field p_0 and the aperture field $H = 2Z_-$,

$$\mathbf{q}_1 = -\frac{H^3}{12}\boldsymbol{\nabla} p_1 - \frac{1}{2240}[\boldsymbol{\nabla}(\boldsymbol{\nabla} p_0)^2 H^7 + 4\,\boldsymbol{\nabla} p_0 (\boldsymbol{\nabla} p_0 \cdot \boldsymbol{\nabla} H) H^6]. \tag{10}$$

Relation (10) is called the Oseen–Poiseuille equation, for it gives the first in-plane inertial correction to the lubrication Darcy–Poiseuille flux. The relationship between inertial effects and the Reynolds pressure field p_0 as well as between inertial effects and the aperture field H is far from being simple even in two dimensions. The flow incompressibility imposes that this in-plane inertial correction $\mathbf{q}_1$ is divergence free, so that the pressure correction p_1 satisfies

$$\boldsymbol{\nabla} \cdot (H^3 \boldsymbol{\nabla} p_1) = -\frac{3}{560}\boldsymbol{\nabla} \cdot [\boldsymbol{\nabla}(\boldsymbol{\nabla} p_0)^2 H^7 + 4\,\boldsymbol{\nabla} p_0 (\boldsymbol{\nabla} p_0 \cdot \boldsymbol{\nabla} H) H^6]. \tag{11}$$

As expected from the perturbation expansion, the pressure correction satisfies the same heterogeneous two-dimensional Poisson problem as p_0 [Eq. (5)] but with a nontrivial right-hand side depending on the leading-order pressure p_0. Section III describes the numerical method used for solving this problem.

To complete this section, we need to calculate the first correction w_1 to the vertical velocity field. The procedure is similar to that used for $\mathbf{u}_1$. The calculation is cumbersome but a useful factorization can be obtained from Eq. (11). The final result reads

$$w_1 = -z(z^2 - Z_-^2)\left\{ \frac{-\,\boldsymbol{\nabla} p_1 \cdot \boldsymbol{\nabla} Z_-}{2Z_-} + \mathcal{P}_{13}\left[\boldsymbol{\nabla} \otimes \boldsymbol{\nabla} p_0 : \boldsymbol{\nabla} \otimes \boldsymbol{\nabla} p_0 - \frac{\boldsymbol{\nabla}(\boldsymbol{\nabla} p_0 \cdot \boldsymbol{\nabla} Z_-) \cdot \boldsymbol{\nabla} p_0}{Z_-} \right] - \mathcal{P}_{14}(\boldsymbol{\nabla} p_0 \cdot \boldsymbol{\nabla} Z_-)^2 - \mathcal{P}_{15}\boldsymbol{\nabla}(\boldsymbol{\nabla} p_0)^2 \cdot \boldsymbol{\nabla} Z_- \right\}, \tag{12}$$

where "⊗" and ":" represent the tensorial product and the double contraction, respectively. The analytical polynomial dependence in the vertical direction z is given by

$$\mathcal{P}_{13}(z) = \frac{1}{840}(z^2 - Z_-^2)(z^2 - 5Z_-^2),$$

$$\mathcal{P}_{14}(z) = \frac{1}{840Z_-^2}(5z^4 - 2z^2Z_-^2 + 109Z_-^4), \tag{13}$$

$$\mathcal{P}_{15}(z) = \frac{Z_-}{120}(z^2 + 3Z_-^2).$$

The vertical velocity component obtained in Eq. (12) fulfills the expected antisymmetric vertical profile in the (x,y,z) coordinates. Using Eqs. (9) and (12), we have checked that the perturbed flow $\mathbf{U}_1=(u_1,v_1,\epsilon w_1)$ is divergence free.

B. Weak disorder asymptotic expansion

The purpose of this section is to obtain an approximate analytical expression for the inertial pressure correction in the limit where the amplitude of the aperture variations is weak. This analysis will be helpful to validate the numerical procedure described in Sec. III and used to solve the inertial pressure and velocity corrections [Eqs. (11) and (12)]. It will also be used to investigate the macroscopic effects of inertia in Sec. IV. Such a solution is obtained for aperture distributions of the form $Z_-=\langle H\rangle(1+\sigma\delta_z)/2$ in the limit where the relative aperture variations σ are small ($\sigma \ll 1$) and where δ_z is a normal-centered (i.e., $\langle\delta_z\rangle=0$, $\langle\delta_z^2\rangle=1$) periodic function in the x and y directions. The relevance of this approximation has been suggested by previous experimental measurements[24] for fractures.

The successive pressure corrections are expanded with the small parameter σ so that

$$p_0 = p_0^{(0)} + \sigma p_0^{(1)} + \sigma^2 p_0^{(2)} + \cdots,$$
$$p_1 = p_1^{(0)} + \sigma p_1^{(1)} + \sigma^2 p_1^{(2)} + \cdots, \tag{14}$$

where $p_0^{(n)}$ and $p_1^{(n)}$ denote the nth-order corrections in σ to p_0 and p_1, respectively. Introducing this expansion in Eqs. (5) and (11) leads to

$$\Delta p_0^{(0)} = 0, \tag{15}$$

$$\Delta p_1^{(0)} = 0, \tag{16}$$

$$\Delta p_0^{(1)} = -3\,\boldsymbol{\nabla}\,\delta_z\cdot\boldsymbol{\nabla}\,p_0^{(0)}, \tag{17}$$

$$\Delta p_1^{(1)} = -3\,\boldsymbol{\nabla}\,\delta_z\cdot\boldsymbol{\nabla}\,p_1^{(0)} - \frac{3}{280}\langle H\rangle^4\,\boldsymbol{\nabla}\cdot\{[\boldsymbol{\nabla}p_0^{(0)}\cdot\boldsymbol{\nabla}\,]\boldsymbol{\nabla}\,p_0^{(1)} + 2\,\boldsymbol{\nabla}\,p_0^{(0)}[\boldsymbol{\nabla}p_0^{(0)}\cdot\boldsymbol{\nabla}\,\delta_z]\}, \tag{18}$$

$$\Delta p_0^{(2)} = -3\,\boldsymbol{\nabla}\,\delta_z\cdot\boldsymbol{\nabla}\,p_0^{(1)} + 3\delta_z\,\boldsymbol{\nabla}\,\delta_z\cdot\boldsymbol{\nabla}\,p_0^{(0)}. \tag{19}$$

Solving analytically Eqs. (15)–(19) turns out to be extremely difficult in the general case and this is why we will restrict our study. We next consider situations where a macroscopic pressure gradient is imposed across the channel. Furthermore, we assume that the representative elementary volume (REV) associated with the typical correlation length of the aperture variations δ_z is small compared to the problem scale L and in the following $\delta_z(\mathbf{r})$ is a Gaussian random field. This hypothesis has also been confirmed by experimental observations.[25] According to the ergodic hypothesis, the probability average is also identified with the spatial average $\langle\,\rangle$ in an infinite domain. The aperture field is considered as being stationary, so that the correlation function of the aperture $\langle\delta_z(\mathbf{r}+\mathbf{r}')\delta_z(\mathbf{r}')\rangle=\rho(\mathbf{r})$ only depends on the relative two-point vector $\mathbf{r}$. All the corrections to $p_0^{(0)}$ are periodic, and therefore are more easily handled in their spectral form. Hereafter $\tilde{p}_0^{(n)}$ and $\tilde{p}_1^{(n)}$ stand for the result of the Fourier transform of $p_0^{(n)}$ and $p_1^{(n)}$, respectively. Boundary conditions must be specified for the harmonic problem (15). When the velocity field is periodic in the two x and y directions, the resulting pressure includes a macroscopic pressure gradient $\boldsymbol{\nabla}P$ equal to the leading-order pressure gradient, $\boldsymbol{\nabla}p_0^{(0)}=\langle\boldsymbol{\nabla}p_0^{(0)}\rangle=\langle\boldsymbol{\nabla}p_0\rangle=\boldsymbol{\nabla}P$. Hence, the periodic solution of the harmonic problem (16) $p_1^{(0)}$ fulfills a zero averaged pressure gradient $\langle\boldsymbol{\nabla}p_1^{(0)}\rangle=0$ and allows to set $p_1^{(0)}=0$. Inserting these expressions into (17) and (18) and rewriting Eqs. (15) and (16) in the Fourier space lead to

$$-k^2\tilde{p}_0^{(1)} = -3i\mathbf{k}\cdot\boldsymbol{\nabla}\,P\tilde{\delta}_z, \tag{20}$$

$$-k^2\tilde{p}_1^{(1)} = -\frac{3}{280}\langle H\rangle^4\{i\mathbf{k}\cdot[\boldsymbol{\nabla}P\cdot i\mathbf{k}\otimes i\mathbf{k}\tilde{p}_0^{(1)}] + 2i\mathbf{k}\cdot[\boldsymbol{\nabla}P(\boldsymbol{\nabla}P\cdot i\mathbf{k}\tilde{\delta}_z)]\}, \tag{21}$$

where $\mathbf{k}$ is the wave vector and $\tilde{\delta}_z$ is the Fourier transform of δ_z. Using Eq. (20), $\tilde{p}_1^{(1)}$ can be expressed from Eq. (21) and gives

$$\tilde{p}_1^{(1)} = \frac{3}{280}\langle H\rangle^4\tilde{\delta}_z\frac{\mathbf{k}\otimes\mathbf{k}}{k^2}:\boldsymbol{\nabla}\,P\otimes\,\boldsymbol{\nabla}\,P. \tag{22}$$

This last equation gives an analytical spectral representation of the first correction to the pressure field in a weak disorder approximation. It is used in Sec. III to check the numerical code and to compute the impact of the first inertial correction at the macroscopic scale.

III. NUMERICAL COMPUTATIONS

A. Solving two-dimensional Oseen–Poiseuille equations

In this section we describe a numerical method for solving the asymptotic two-dimensional problems obtained in Sec. II. A spectral element method[26] is used to discretize the equations and to evaluate the pressure, velocity, stream function, and their successive inertial corrections previously described. The fields are approximated with $N_x\times N_y$ order polynomials in the x and y directions, respectively, and the interpolant of each field is numerically represented with its $(N_x+1)\times(N_y+1)$ values at the Gauss–Lobatto–Legendre nodes.[27] One advantage of this choice lies in the high-order

Gauss–Lobatto quadrature that can be used for the evaluation of the integrals arising from the variational formulation of the problem. As for Eqs. (5) and (11), the corresponding linear problem is (in general) a nonhomogeneous Laplacian which has the form discussed by Azaïez, Bergeon, and Plouraboué[28] for flows in heterogeneous porous media. Here, it is solved with a conjugate gradient method preconditioned by the Laplacian. This last operator is inverted with a direct solver by means of a tensor product method.[29]

The comparison of the size of the REV and that of the numerical domain defines two problems with different boundary conditions. If the two domains are of the same order, Dirichlet or Neumann boundary conditions are used to take into account realistic boundary conditions and this case falls in the numerical treatment that we described in the last paragraph. On the other hand, if the REV is small compared to the numerical domain, the corrections to the imposed pressure gradient are periodic and are expanded in Fourier series instead of polynomials. In this case, we impose a uniform mean pressure gradient along the x direction. We then solve a periodic problem in both x and y directions for the pressure deviation to this uniformly increasing imposed pressure. Hence in this case p_0 is only periodic along the y direction. However, it should be noted that even if the aperture $H=2Z_-$ and the corrections to p_0 and $\mathbf{u}_0$ are periodic, the corresponding stream functions Ψ_0 and its inertial correction Ψ are not necessarily periodic. Since these fields are solutions of a Laplacian equation with Neumann boundary conditions, the problem must be rewritten on a Gauss–Lobatto–Legendre grid prior to being solved.

B. Numerical tests

1. Validation with analytic two-dimensional solutions

To check the accuracy of the two-dimensional code, an analytic solution is compared with its numerical approximation. Substituting $\boldsymbol{\nabla} P$ by $\mathbf{e_x}$ in Eq. (22) gives

$$\tilde{p}_1^{(1)} = \frac{3}{280}\langle H\rangle^4(\cos\theta)^2\tilde{\delta}_z, \tag{23}$$

where θ is the azimuthal angle in the Fourier space defined by $\cos\theta=\mathbf{e}_x\cdot\mathbf{k}/\|\mathbf{k}\|$. Transforming back to the physical space, one obtains the solution expressed in cylindrical coordinates (r,ϕ),

$$p_1^{(1)} = \frac{3}{280}\left[-\frac{1}{2\pi}\frac{\cos(2\phi)}{r^2}+\frac{\delta(0)}{2}\right] * \delta_z(r,\phi,\phi_0), \tag{24}$$

where ϕ is the azimuthal angle, ϕ_0 is the angle between vectors $\mathbf{k}_0$ and $\mathbf{e}_x$, $\cos\phi_0=\mathbf{k}_0\cdot\mathbf{e}_x/\|\mathbf{k}_0\|$, and "$*$" is the convolution product. This relation shows that $p_1^{(1)}$ varies linearly with the aperture spatial variations, a direct consequence of a first-order perturbative expansion. In the case of a simple sinusoidal aperture perturbation, $\delta_z(r,\phi,\phi_0)=\cos(\mathbf{k}_0\cdot\mathbf{r})$, one gets

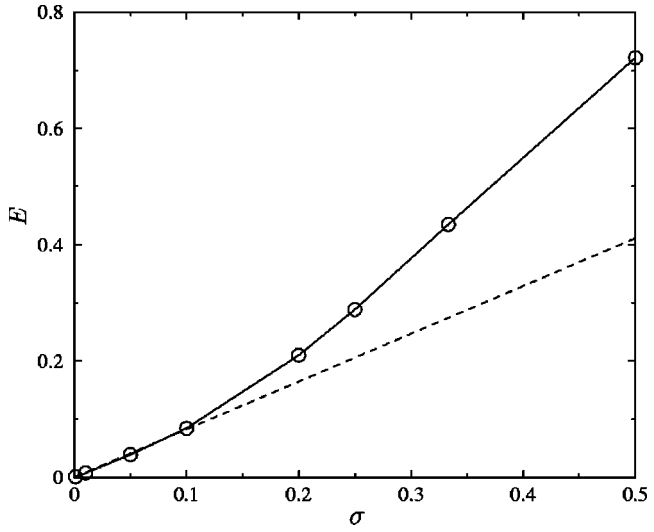

FIG. 1. Relative error $E=\|p-p_0^0-\sigma(p_0^1+\epsilon\,\mathrm{Re}\,p_1^1)\|$ between the numerical pressure p and its asymptotic estimates established in (20) and (23).

$$p_1^{(1)}(r,\phi) = \frac{3}{280}(\cos\phi_0)^2\cos(\mathbf{k}_0\cdot\mathbf{r}). \tag{25}$$

To compare the numerical solution with the analytical expression, we choose $\delta_z=\cos(x+y)$ leading to $p_1^{(1)}=3\cos(x+y)/560$. Figure 1 displays the relative error between $p_1^{(1)}$ and its numerical approximation and shows that it approaches zero as $\sigma\to 0$. Therefore, this result validates numerical procedure used for approximating Eq. (18). Moreover, we know that the correction to the first order is $O(\sigma^2)$, with a corresponding relative error of $O(\sigma)$. This result is consistent with the linear behavior effectively observed in Fig. 1 when $\sigma\ll 1$.

2. Discussion about the resulting inertial perturbation

In this subsection we shall discuss the structure of the inertial corrections to the zero Reynolds number lubrication streamlines. As Sec. II, we consider a simple perturbation $\delta_z=\cos(x+y)+\cos(x-y)$ of the aperture H, but the amplitude σ of this perturbation will not necessarily be small in this subsection. Figure 2(b) displays the lubrication streamlines Ψ_0 associated with the divergence-free flux $\mathbf{q}_0$ computed from inverting its relation with the flux $\mathbf{q}_0$,

$$\Delta\boldsymbol{\Psi}_0 = \nabla\times\mathbf{q}_0, \tag{26}$$

where $\Psi_0=(0,0,\Psi_0)$. The inversion of the Laplacian operator is carried out with a direct method using periodic boundary conditions in y directions and Neumann boundary conditions along x direction. From the superposition of the stream function and the aperture field $H(x,y)$ in the gray level on Fig. 2(a), it can be observed, as expected, that the flux is maximal in regions where the aperture is the largest. The symmetry invariances of the chosen aperture corrugation are those of the group D_4, the symmetry group of the square. This group has eight elements and is generated by S_x (or S_y) and Π_{xy} (or Π_{yx}) which are reflections with respect to $x=\pi$ (or $y=\pi$) and $x-y=\pi$ (or $x+y=\pi$), respectively. The symmetries of the noninertial pressure p_0 which satisfies Eq. (5)

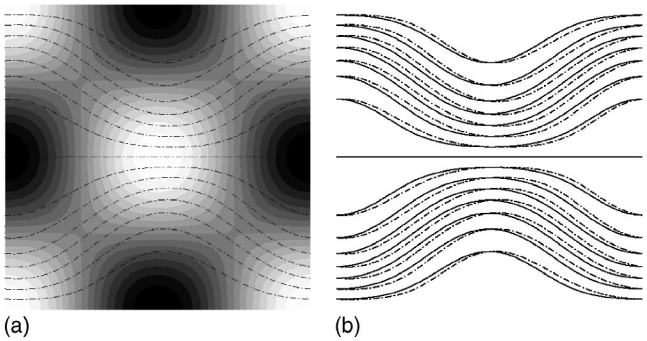

FIG. 2. (a) The dash-dotted lines refer to the streamlines associated with the mean flux $\Psi=\Psi_0+\epsilon\,\mathrm{Re}\,\Psi_1$ while the local distance Z_- between the two surfaces is represented in gray scale from black for the minimum to white for the maximum where $Z_-=\epsilon\{1+\sigma[\cos(x+y)+\cos(x-y)]\}$, with $\sigma=0.30$ and $\epsilon=2\pi/5$. (b) Comparison between noninertial streamline Ψ_0 (continuous lines) and streamlines $\Psi=\Psi_0+\epsilon\,\mathrm{Re}\,\Psi_1$ associated with inertial effects (dash-dotted lines).

not only depend on the symmetries of $H(x,y)$ (i.e., those of δ_z) but also on boundary conditions. Because the boundary conditions of the pressure p_0 are different along $x=0,2\pi$, and $y=0,2\pi$, the relevant symmetry is given by the group D_2 generated by S_x and S_y. As can be seen on Fig. 2(b), the noninertial flow (continuous lines) is D_2 invariant. Now, including some inertia in the flow breaks some of these symmetry invariances. As observed on the same figure, the total stream function $\Psi=\Psi_0+\epsilon\,\mathrm{Re}\,\Psi_1$ represented with the dotted line is not S_x symmetric any more. The broken symmetries result from the physical effects that streamlines keep a memory of the flow meandering with a delayed response typical of inertia. The effect of inertia can better be identified by examining the inertial correction to the stream function Ψ_1, while varying the amplitude of the perturbation σ. The inertial correction Ψ_1 is computed from its relation to $\mathbf{q}_1$ similar to (26) with periodic boundary conditions. As observed on Fig. 3(a), when σ is very small, the stream function displays a quadrupolar structure. From the orthogonality between the stream function and the pressure, this property is expected from the quadrupolar structure of the pressure field obtained from (25) {i.e., $p_1=3\sigma[\cos(x+y)+\cos(x-y)]/560$, in the limit of $\sigma\ll 1$ when $\delta_z=\cos(x+y)+\cos(x-y)$}. In this case p_1 and Ψ_1 are S_x and S_y antisymmetric, as can be observed on Fig. 3. When increasing the parameter σ the stream function Ψ_1 still display a quadrupolar symmetry, but a more complex shape with secondary maximum [Figs. 3(b)–3(d)] results from an increased perturbation σ. These effects illustrate on a simple example the physics of inertial effects, as well as the rich behavior of the flow field structure on a very simple perturbation.

3. Comparison with full three-dimensional Navier–Stokes computations

The numerical simulation of the three-dimensional (3D) Navier–Stokes equations employs a projection method based on a spectral spatial discretization already described in Sec. III A. After the nonlinear terms have been computed explicitly via second-order extrapolation, a Poisson problem is formulated for the pressure using the boundary conditions pro-

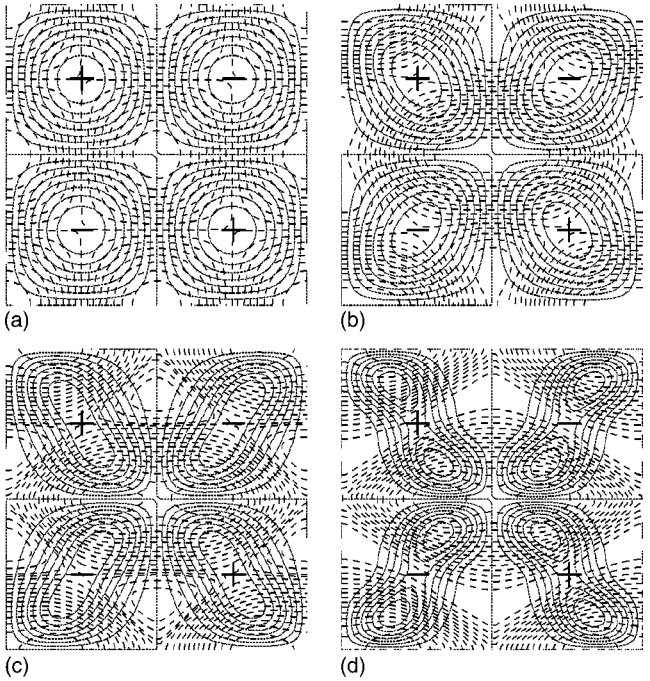

FIG. 3. Inertial correction Ψ_1 to the stream function (dotted lines) and inertial correction to the pressure p_1 (dashed lines) for $Z=\epsilon\{1+\sigma[\cos(x+y)+\cos(x-y)]\}$, with $\epsilon=2\pi/5$ for four different values of σ: (a) $\sigma=0.0005$, (b) $\sigma=0.15$, (c) $\sigma=0.30$, and (d) $\sigma=0.45$.

posed by Karniadakis, Israeli, and Orszag.[30] This Poisson problem, as well as the Helmholtz problems which incorporate the viscous terms and constitute the final implicit step of the scheme, is solved using a variational formulation.[31] Most of the computational time is spent in the inversion of the pressure and velocity problems. The corresponding algebraic systems are solved in the hexahedral element of reference $\hat{\Omega}=[-1,1]^3$ in which all function evaluations are carried out. These evaluations require the mapping from $\hat{\Omega}$ to the fracture and its Jacobian which are both analytically known. In $\hat{\Omega}$ the discrete Laplacian takes the form of a tensor product sum of one-dimensional stiffness and mass matrix associated with the three spatial directions. If the aperture is constant, this sum has three terms and can be easily rewritten so that each term in the sum involves only one spatial direction. This way, the algebraic linear system can be inverted with a direct method based on a diagonalization procedure.[29] Such a transformation is not possible in the present case where the fracture is a nontrivially deformed hexahedral element. We therefore use a conjugate gradient method preconditioned by a homogenized version of the Laplacian as described in Ref. 28. This preconditioning turns out to be very efficient compared with the the Laplacian when the aspect ratio of the initial problem is large or the variations of the aperture are small. We have used the code to compute the steady states increasing the Reynolds number (defined in Sec. II A) from 0 to 200 with a step of 5.

For Reynolds in [0,200], the Oseen–Poiseuille asymptotic and full three-dimensional Navier–Stokes flows are compared in Fig. 4 for a simple one-mode geometry $Z_-(x,y)=\epsilon\{1+\sigma[\cos(x+y)+\cos(x-y)]\}$ with $\sigma=0.15$, ϵ

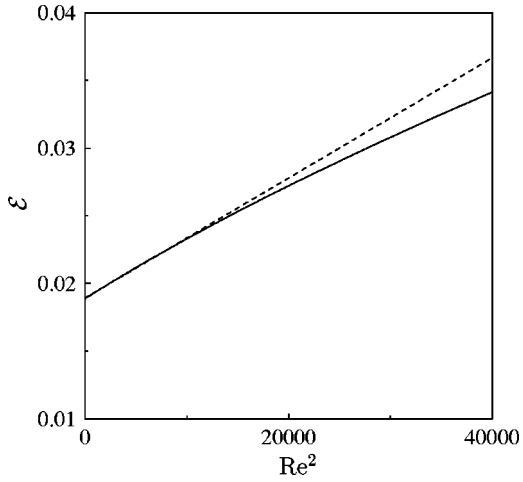

FIG. 4. Continuous line: Evolution with the Reynolds number of the relative error $\varepsilon=\|\mathbf{u}_{\mathrm{NS}}(\mathrm{Re})-\mathbf{u}_{\mathrm{As}}(\mathrm{Re})\|/\|\mathbf{u}_{\mathrm{NS}}(\mathrm{Re})\|$, where $\mathbf{u}_{\mathrm{NS}}$ and $\mathbf{u}_{\mathrm{As}}$ refer to the velocity field obtained with the Navier–Stokes equations and the first-order asymptotic approximation, respectively. The dashed line refers to the approximation by means of a linear regression on the values obtained for Re $\in[0,100]$. The aperture is $Z_{-}(x,y)=\epsilon\{1+\sigma[\cos(x+y)+\cos(x-y)]\}$ with $\sigma=0.15$ and $\epsilon=2\pi/10$. Periodic boundary conditions are imposed in the x and y directions and no slip along the rough surfaces. Resolution is $64\times32\times21$.

$=2\pi/10$, and periodic boundary conditions in the x and y directions. The figure displays the variations of the difference between the two velocity fields with the Reynolds number. The results indicate that the part neglected when approximating the Navier–Stokes flows to the first order varies quadratically with the Reynolds number. This behavior was expected and also proves that the asymptotic approximation correctly captures the first inertial correction: if the approximation had not been consistent, the figure would have displayed a linear dependence with the Reynolds number. Examination of Fig. 4 also shows that the error arising from second-order $O(\epsilon^2\,\mathrm{Re}^2)$ inertial contributions remains smaller than those existing at Re=0. As a matter of fact at Re=0 there is an error of 1.8%. This is consistent with an expected error coming from Stokes corrections of order ϵ^2 when the aspect ratio of the chosen surfaces ϵ is 0.1, so that ϵ^2 gives 1% errors. It is also interesting to compare linear inertial corrections to quadratic ones from direct numerical simulations. For example, at Re=50 we found that linear inertial corrections represent (i.e., their quadratic norm contribution) 1% of the total flow field, whereas quadratic corrections represent only 0.1%. The differences in the velocity fields between the Stokes flow and its lubrication approximation are illustrated in Figs. 6–8(a) and 8(b) for different boundary conditions in the y direction: no-slip, stress-free ($\partial u/\partial x=\partial w/\partial z=v=0$) and periodic velocity boundary conditions, respectively. It is completed with Figs. 6–8(c) and 8(d) where the inertial effects for the Navier–Stokes and Oseen–Poiseuille asymptotic flows are compared for Re=50. For periodic boundary conditions, the figures show that the velocity fields are very similar. As observed from Fig. 4, the differences between Stokes and lubrication flows are larger than those between the inertial corrections. In the case of nonperiodic boundary conditions, the inertial effects increase the spatial extension

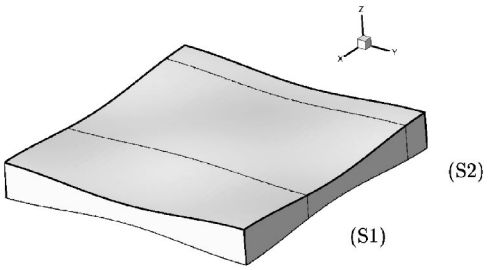

FIG. 5. View of the fracture geometry and surfaces $S1$ and $S2$ used for Figs. 6–8.

of the lateral boundary layers proportionally to $\mathrm{Re}^{1/2}$. Figure 6 shows that for Re=50 this extension is twice the mean aperture. Therefore, even if the proposed asymptotic is interesting for describing the inertial flows far from lateral boundaries, it should be kept in mind that boundary layer effects are also significantly increased by inertia.

In Fig. 9, the relative contribution of the inertial corrections to the lubrication approximation is presented as a function of the Reynolds number and for the geometry used in the periodic case (the configuration used for Fig. 4). At Re =100, the relative contribution is 20% for the velocity field and becomes 40% at Re=200. This indicates that the first inertial contribution introduces a significant difference in the lubrication approximation. The asymptotic modeling of inertial effect thus provides an interesting approximation for flows confined in between two rough surfaces where inertial contribution to the velocity field is still small for Reynolds number as large as 100.

IV. MACROSCOPIC INERTIAL EFFECTS

Equation (10) describes the first-order nonlinear relation between the flux $\mathbf{q}$ and the pressure gradient $\boldsymbol{\nabla}p$ on the microscopic length scale. In this section, we address the impact of this first inertial correction on the macroscopic flux $\langle\mathbf{q}\rangle\equiv\mathbf{Q}$ due to an imposed pressure gradient $\langle\boldsymbol{\nabla}p\rangle\equiv\boldsymbol{\nabla}P$. We focus on situations where the macroscopic pressure gradient

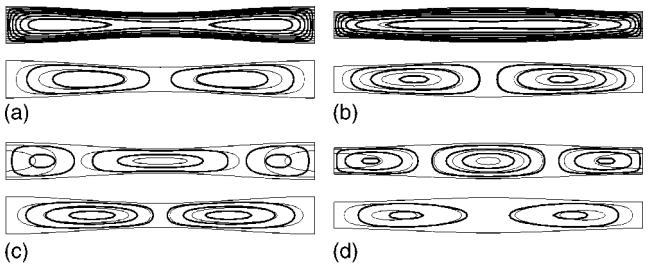

FIG. 6. [(a) and (b)] Comparison of the full 3D Navier–Stokes flow and the asymptotic approximation at Re=0. [(c) and (d)] Same as (a) and (b) but for the inertial correction at Re=50. The bold lines refer to Navier–Stokes solutions and the thin lines to first- or zeroth-order asymptotic approximation. (a)–(d) depict the isovalues of u (top) and v (bottom) on two planes [(a) and (c)] $x=\pi/4$ (surface $S1$) and [(b) and (d)] $x=21\pi/32$ (surface $S2$). The two surfaces $S1$ and $S2$ are presented in Fig. 5 along with the fracture defined by $z(x,y)=\epsilon[1+\sigma\cos(x+y)]$ with $\sigma=0.15$ and $\epsilon=2\pi/10$ and $0\leqslant x,y\leqslant2\pi$. Stress free-boundary conditions are used for the velocity along the vertical lateral side walls for the asymptotic computation and no slip for the Navier–Stokes. Resolution is $32\times41\times21$.

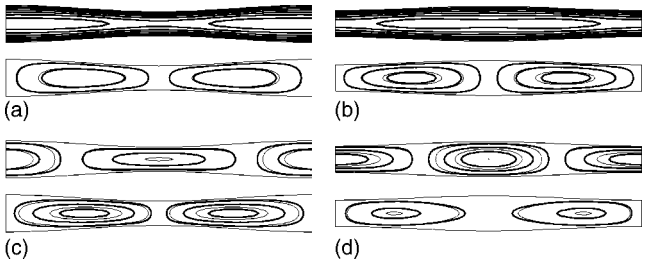

FIG. 7. [(a) and (b)] Comparison of the full 3D Navier–Stokes flow and the asymptotic approximation at Re=0. [(c) and (d)] Same as (a) and (b) but for the inertial correction at Re=50. The bold lines refer to Navier–Stokes solutions and thin lines to first- or zeroth-order asymptotic approximation. (a)–(d) depict the isovalues of u (top) and v (bottom) on two planes [(a) and (c)] $x=\pi/4$ (surface $S1$) and [(b) and (d)] $x=21\pi/32$ (surface $S2$). The two surfaces $S1$ and $S2$ are presented in Fig. 5 along with the fracture defined by $z(x,y)=\epsilon[1+\sigma\cos(x+y)]$ with $\sigma=0.15$ and $\epsilon=2\pi/10$ and $0\leqslant x,y\leqslant 2\pi$. Stress free-boundary conditions are used for the velocity along the vertical lateral side walls for the asymptotic computation and for the Navier–Stokes. Resolution is $32\times41\times21$.

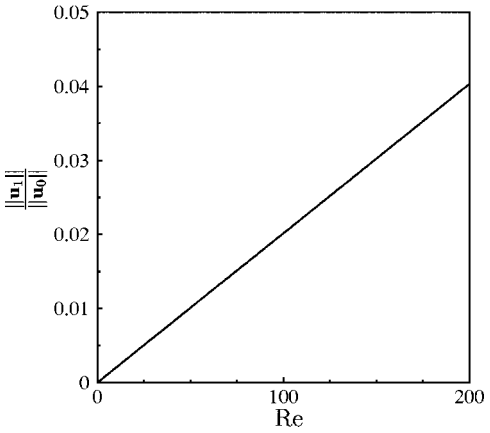

FIG. 9. Evolution with the Reynolds number of the first inertial relative correction $\|\mathbf{u}_1\|/\|\mathbf{u}_0\|$, where $\mathbf{u}(\mathrm{Re})=\mathbf{u}_0+\epsilon\,\mathrm{Re}\,\mathbf{u}_1$. The aperture is $Z_-(x,y)=\epsilon\{1+\sigma[\cos(x+y)+\cos(x-y)]\}$ with $\sigma=0.15$ and $\epsilon=2\pi/10$. Periodic boundary conditions are imposed in the x and y directions and no slip along the rough surfaces. Resolution is $64\times32\times21$.

is imposed. The macroscopic flux $\mathbf{Q}$ is decomposed into a Reynolds contribution $\mathbf{Q}_0$ and a first inertial correction $\mathbf{Q}_1$ with $\mathbf{Q}=\mathbf{Q}_0+\mathrm{Re}\,\epsilon\mathbf{Q}_1$.

In a general case, solving Eq. (11) is far from simple. Here, two complementary techniques are presented: perturbative spectral methods and volume averaging technique. The perturbative spectral method permits to obtain analytically the inertial macroscopic flux for any general (periodic) permeability field provided that it weakly fluctuates around its mean value. The volume averaging technique allows to evaluate the macroscopic flux given a specified permeability field after solving a closure problem written on a REV.

A. Weak disorder perturbative spectral method

In Sec. II B, we obtained the first-order term for the pressure perturbation. To complete our calculation and express $\mathbf{Q}_1$, we need to evaluate all successive corrections in σ to $\tilde{p}_1$. Following the expansion carried out in Sec. II B, it is easy to see that the expression for $\mathbf{q}_1^{(2)}$ requires the evaluation

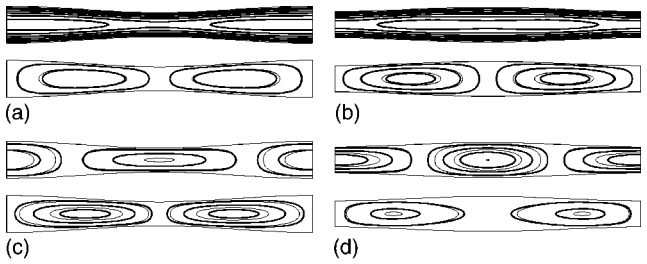

FIG. 8. [(a) and (b)] Comparison of the full 3D Navier–Stokes flow and the asymptotic approximation at Re=0. [(c) and (d)] Same as (a) and (b) but for the inertial correction at Re=50. The bold lines refer to Navier–Stokes solutions and the thin lines to first- or zeroth-order asymptotic approximation. (a)–(d) depict the isovalues of u (top) and v (bottom) on two planes [(a) and (c)] $x=\pi/4$ (surface $S1$) and [(b) and (d)] $x=21\pi/32$ (surface $S2$). The two surfaces $S1$ and $S2$ are presented in Fig. 5 along with the fracture defined by $z(x,y)=\epsilon[1+\sigma\cos(x+y)]$ with $\sigma=0.15$ and $\epsilon=2\pi/10$ and $0\leqslant x,y\leqslant 2\pi$. Periodic boundary conditions are used for the velocity along the vertical lateral side walls for the asymptotic computation and for the Navier–Stokes. Resolution is $64\times64\times41$.

of $p_0^{(2)}$ [while the evaluation of $p_1^{(2)}$ is not necessary since $\langle\boldsymbol{\nabla}p_1^{(2)}\rangle=0$]. Again this is achieved in the Fourier space. The solution of (19) can be obtained from Eq. (20) and leads to

$$\tilde{p}_0^{(2)}=\frac{9i}{k^2}\int(\mathbf{k}-\mathbf{k}')\cdot\left(3\frac{\mathbf{k}'\otimes\mathbf{k}'}{k'^2}+1\right)\tilde{\delta}_z(\mathbf{k}')\tilde{\delta}_z(\mathbf{k}-\mathbf{k}')d\mathbf{k}'\cdot\boldsymbol{\nabla}P, \tag{27}$$

where "·" is the contraction, the upper tilde is the Fourier transform of previously defined fields, and 1 represents the identity tensor. We now wish to compute the macroscopic inertial flux $\langle\mathbf{q}_1\rangle=\langle H\boldsymbol{\nabla}p_1\rangle$. Using relations (22) and (27) and collecting equal powers of σ, the averaging leads to the following expressions:

$$\langle\mathbf{q}_1^{(0)}\rangle=\mathbf{0}, \tag{28}$$

$$\langle\mathbf{q}_1^{(1)}\rangle=\mathbf{0}, \tag{29}$$

$$\langle\mathbf{q}_1^{(2)}\rangle=\frac{3i\langle H\rangle^3}{280}\int\frac{\mathbf{k}\otimes\mathbf{k}\otimes\mathbf{k}}{k^2}\tilde{\rho}(\mathbf{k})d\mathbf{k}:\boldsymbol{\nabla}P\otimes\boldsymbol{\nabla}P, \tag{30}$$

where $\tilde{\rho}(\mathbf{k})=|\tilde{\delta}_z(\mathbf{k})|^2$ is the power spectrum of the aperture fluctuations which is equal to the Fourier transform of the correlation function. Since the aperture field is stationary, $\rho(\mathbf{r})=\rho(-\mathbf{r})$, and therefore $\tilde{\rho}(\mathbf{k})=\tilde{\rho}(-\mathbf{k})$. The term in the integral of Eq. (30) is an odd function of $\mathbf{k}$ and therefore $\langle\mathbf{q}_1^{(2)}\rangle=\mathbf{0}$. Hence, up to the second order of a weak disordered expansion, the inertial pressure field does not produce any contribution to the macroscopic flux $\mathbf{Q}$. Since by symmetry the third-order contributions also vanish, $\mathbf{Q}_1=\mathbf{0}$ up to the fourth-order σ contributions. To further investigate this result, we next turn to the volume averaging technique.

B. Volume averaging technique

We shall consider the aperture as being a deterministic periodic field among the REV. The pressure field is then decomposed into a macroscopic pressure P and deviation p', $p=P+p'$. Consequently, we assume that the correction p' to

the macroscopic pressure field P is periodic in the x and y directions. At the REV scale, the macroscopic pressure gradient is supposed to be constant. Following Quintard and Whitaker[32] the deviation is decomposed along the constant macroscopic pressure gradient ∇P. Including inertial effects, the deviation p' can then be written as

$$p' = \mathbf{b}_0 \cdot \nabla P + \mathrm{Re}\,\epsilon \mathbf{b}_1 : \nabla P \otimes \nabla P, \tag{31}$$

where $\mathbf{b}_0$ is a two-component closure vector field and $\mathbf{b}_1$ is a 2×2 closure tensor field which must be evaluated numerically. The inertial contribution to the macroscopic flux $\mathbf{Q}_1$ is then directly related to the second closure tensor $\mathbf{b}_1$ after averaging the local flux/pressure gradient relation. We obtain

$$\mathbf{Q}_1 = -\frac{1}{12}\langle H^3 \nabla \mathbf{b}_1 \rangle : \nabla P \otimes \nabla P, \tag{32}$$

where $\nabla \mathbf{b}_1$ is a third-order tensor. Using the pressure decomposition (31) in relation (5) one gets the first noninertial closure problem,

$$\nabla \cdot [H^3(\nabla \mathbf{b}_0 + 1)] = \mathbf{0}, \tag{33}$$

where $\nabla \mathbf{b}_0$ is a second-order tensor. The closure problem (33) has been already obtained by Quintard and Whitaker[32] in the context of heterogeneous porous media and is discussed by Prat, Plouraboué, and Letalleur[23] for flows between rough surfaces. Equation (33) has to be solved with periodic boundary conditions for the vector field $\mathbf{b}_0$ and aperture field H. Moreover, since the solution is defined up to a constant vector, the condition $\langle \mathbf{b}_0 \rangle = \mathbf{0}$ is prescribed (arising from the decomposition $\langle p = P + p' \rangle = P$). The second inertial closure problem for the second closure tensor $\mathbf{b}_1$ is obtained after inserting decomposition (31) in Eq. (11). The right-hand side of Eq. (11) can be simplified after observing that

$$\nabla (\nabla p_0)^2 = [2 \nabla \otimes \nabla \mathbf{b}_0 + \nabla (\nabla \mathbf{b}_0)^2] : \nabla P \otimes \nabla P, \tag{34}$$

where $\mathbf{b}_0^2 = \mathbf{b}_0 \cdot \mathbf{b}_0$ is the norm of vector $\mathbf{b}_0$ and

$$\nabla p_0 (\nabla p_0 \cdot \nabla H) = [(1 + \nabla \mathbf{b}_0) \otimes (1 + \nabla \mathbf{b}_0) \cdot \nabla H] : \nabla P \otimes \nabla P. \tag{35}$$

The equation for the inertial 2×2 deviation matrix $\mathbf{b}_1$ can therefore be written independently from the imposed macroscopic pressure gradient,

$$\nabla \cdot (H^3 \nabla \mathbf{b}_1) = -\frac{3}{560} \nabla \cdot \{H^7 [2 \nabla \otimes \nabla \mathbf{b}_0 + \nabla (\nabla \mathbf{b}_0)^2] + 4H^6 (1 + \nabla \mathbf{b}_0) \otimes (1 + \nabla \mathbf{b}_0) \cdot \nabla H\}. \tag{36}$$

This complicated 2×2 closure problem for the second-order tensor $\mathbf{b}_1$ must be solved numerically for a given permeability field and using periodic boundary conditions and the same average constraint $\langle \mathbf{b}_1 \rangle = \mathbf{0}$ as for the previous closure problem. The solution of this problem has been obtained numerically for a two parameter aperture family, $Z_-(x,y) = 1 + \sigma_1 \cos(x+y) + \sigma_2 \cos(x-y)$. This aperture family generates the base functions for every one-periodic aperture field on the REV. Using the spectral numerical method of Sec. III, we found that for any parameters $(\sigma_1, \sigma_2) \in [0,1[^2$, the third-order tensor $\langle Z_-^3 \nabla \mathbf{b}_1 \rangle$ vanishes. We therefore conclude that the quadratic inertial corrections have zero net flux, $\mathbf{Q}_1 = \mathbf{0}$.

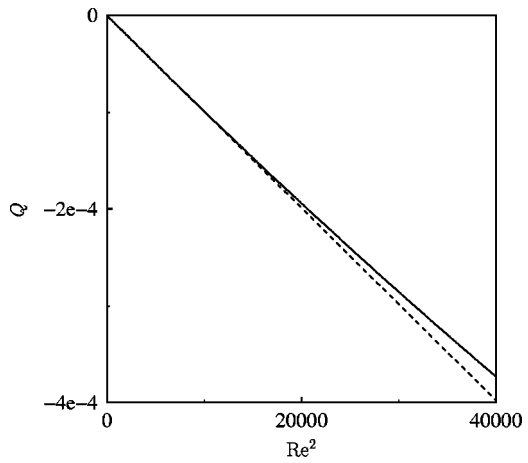

FIG. 10. Continuous line: Evolution of the total flux of the full Navier–Stokes inertial correction $\mathbf{u}(\mathrm{Re}) - \mathbf{u}(\mathrm{Re}=0)$ with the Reynolds number. The dashed line refers to the approximation by a linear regression of the values obtained for $\mathrm{Re} \in [0,100]$. The aperture is $Z_-(x,y) = \epsilon\{1 + \sigma[\cos(x+y) + \cos(x-y)]\}$ with $\sigma = 0.15$ and $\epsilon = 2\pi/10$. Periodic boundary conditions are imposed in the x and y directions and no slip along the rough surfaces. Resolution is $64\times 32\times 21$.

It is then expected that weak-inertial effects produce a cubic macroscopic dependence, as already obtained in the case of porous media.[19] The general form for such a cubic correction can be formally written in its dimensionless version as

$$\mathbf{Q} = \frac{\mathbf{K}}{12} \cdot \nabla P + (\mathrm{Re}\,\epsilon)^2 \mathbf{B} \vdots \nabla P \otimes \nabla P \otimes \nabla P, \tag{37}$$

where $\mathbf{K}$ is a nondimensional second-order permeability tensor and $\mathbf{B}$ is a fifth-order macroscopic inertial tensor. Estimating the detailed dependence of $\mathbf{B}$ on microscopic geometry is far beyond the scope of this paper and would require much larger computational efforts. This law is usually expressed in the porous media literature in the case of imposed flux boundary condition, for which it can very easily be transposed,

$$\nabla P = 12 \mathbf{K}^{-1} \cdot \mathbf{Q} + (\mathrm{Re}\,\epsilon)^2 \mathbf{B}' \vdots \mathbf{Q} \otimes \mathbf{Q} \otimes \mathbf{Q}. \tag{38}$$

This last expression has been numerically evaluated in the case of two-dimensional fracture flows[21] for which it becomes a scalar relation. The range of validity of this regime was found numerically to be rather narrow, confined to Reynolds numbers smaller than unity. These numerical results have nevertheless been obtained for a fracture having large slopes. They should be considered in the light of the accompanying analysis. As a matter of fact it has been shown that inertial effects are revealed through the product of the mean slope and the reduced lubricated Reynolds number for fractures with small slopes—relevant for real fractures.[24] The validity range of cubic inertial effects should thus be much larger for flows through geometries having a small slope. Figure 10 shows the computed flux from the full three-dimensional Navier–Stokes solution in the geometry analyzed in Figs. 6–8. These variations with Re confirm the

quadratic dependence to the cubic correction proposed in (37). The validity range of the observed cubic regime is, as expected, quite large since a deviation of 10% is observed at Reynolds number as large as 200.

V. CONCLUSION

The first inertial correction for a Newtonian fluid flowing between two slowly varying rough surfaces has been analyzed. Two-dimensional Oseen–Poiseuille equations have been obtained relating the inertial correction to the mean flux with the inertial pressure gradient correction and the leading-order lubrication pressure. The velocity field associated with the inertial correction has also been analytically computed as a closed expression of the pressure leading order and inertial correction. As for the Reynolds equations, those inertial corrections necessitate some numerical computation to be solved in complicated geometries. A numerical method has been proposed and validated in the limit of weak disordered aperture fields. The validity range of the proposed asymptotic Oseen–Poiseuille equations has been assessed through direct three-dimensional numerical simulations of Navier–Stokes equations. It has been shown that for $10/\epsilon > \mathrm{Re} \gg \epsilon$, Oseen–Poiseuille approximation gives less than 1% precision on the flow field when the aspect ratio ϵ is smaller than 0.1. The macroscopic influence of weak-inertial effects has also been examined. The inertial corrections to the macroscopic flux when imposing a macroscopic pressure difference have been analyzed. It has been found with two complementary averaging techniques that quadratic weak-inertial effects have no macroscopic influence. Those analyses have been complemented with direct three-dimensional numerical simulation for which a cubic regime has been observed over a wide range of Reynolds numbers.

[1] I. J. Sobey, "Dispersion caused by separation during oscillatory flow through a furrowed channel," Chem. Eng. Sci. **40**, 2129 (1985).
[2] S. W. Jones, O. M. Thomas, and H. Aref, "Chaotic advection by laminar flow in a twisted pipe," J. Fluid Mech. **209**, 335 (1989).
[3] W. R. Dean, "Note on the motion of fluid in a curved pipe," Philos. Mag. **4**, 208 (1927).
[4] W. R. Dean, "The streamline motion of fluid in a curved pipe," Philos. Mag. **5**, 673 (1928).
[5] A. D. Stroock, S. K. W. Dertinger, A. Ajdari, I. Mezic, H. A. Stone, and G. M. Whitesides, "Chaotic mixer for microchannels," Science **295**, 647 (2002).
[6] H. Aref, "Stirring by chaotic advection," J. Fluid Mech. **143**, 1 (1984).
[7] A. D. Stroock, S. K. Dertinger, G. M. Whitesides, and A. Ajdari, "Patterning flows using grooved surfaces," Anal. Chem. **74**, 5306 (2002).
[8] B. Sunden and S. Trollheden, "Periodic laminar flow and heat transfer in a corrugated two dimensional channel," Int. Commun. Heat Mass Transfer **16**, 215 (1989).
[9] H. Zhou, R. E. Khayat, R. J. Matinuzzi, and A. G. Straatman, "On the validity of the perturbation approach for the flow inside weakly modulated channels," Int. J. Numer. Methods Fluids **39**, 1139 (2002).
[10] J. Ashmore, A. E. Hosoi, and H. A. Stone, "The effect of surface tension on rimming flows in a partially filled rotating cylinder," J. Fluid Mech. **479**, 65 (2003).
[11] A. E. Hosoi and L. Mahadevan, "Axial instability of a free-surface front in a partially-filled horizontal rotating cylinder," Phys. Fluids **11**, 97 (1999).
[12] S. P. Lin, "Finite amplitude side-band stability of a viscous film," J. Fluid Mech. **63**, 417 (1974).
[13] W. G. Pritchard, L. R. Scott, and S. J. Tavener, "Numerical and asymptotic methods for certain viscous free-surface flows," Philos. Trans. R. Soc. London, Ser. A **340**, 1 (1992).
[14] S. Ubal, M. D. Giavedoni, and F. A. Saita, "A numerical analysis of the influence of the liquid depth on two-dimensional Faraday waves," Phys. Fluids **15**, 3099 (2003).
[15] H.-C. Chang, E. A. Demekhin, and D. I. Kopelevich, "Nonlinear evolution of waves on a vertically falling film," J. Fluid Mech. **250**, 433 (1993).
[16] P. H. Gaskell, P. K. Jimack, M. Sellier, H. M. Thompson, and M. C. T. Wilson, "Gravity-driven flow of continuous thin liquid films on non-porous substrates with topography," J. Fluid Mech. **509**, 253 (2004).
[17] D. R. Sawyers, M. Sen, and H.-C. Chang, "Heat transfer enhancement in three-dimensional corrugated channel flow," Int. J. Heat Mass Transfer **41**, 3559 (1998).
[18] M. R. Siddique and R. E. Khayat, "Influence of inertia and topography in thin-cavity flow," Phys. Fluids **14**, 1703 (2002).
[19] C. C. Mei and J.-L. Auriault, "Mechanics of heterogeneous porous-media with several spatial scales," Proc. R. Soc. London, Ser. A **426**, 391 (1989).
[20] M. Firdaouss, J.-L. Guermond, and P. Le Quéré, "Nonlinear corrections to Darcy's law at low Reynolds numbers," J. Fluid Mech. **343**, 331 (1997).
[21] E. Skjetne, A. Hansen, and J. S. Gudmundsson, "High-velocity flow in a rough fracture," J. Fluid Mech. **383**, 1 (1999).
[22] E. O. Tuck and A. Kouzoubov, "A laminar roughness boundary-condition," J. Fluid Mech. **300**, 59 (1995).
[23] M. Prat, F. Plouraboué, and N. Letalleur, "Averaged Reynolds equation for flow between rough surfaces in sliding motion," Transp. Porous Media **48**, 291 (2002).
[24] F. Plouraboué, P. Kurowski, J. M. Boffa, J. P. Hulin, and S. Roux, "Experimental study of the transport properties of rough self-affine fractures," J. Contam. Hydrol. **46**, 295 (2000).
[25] F. Plouraboué, P. Kurowski, J. P. Hulin, S. Roux, and J. Schmittbuhl, "Aperture of rough cracks," Phys. Rev. E **51**, 1675 (1995).
[26] C. Canuto, M. Y. Hussaini, A. Quarteroni, and T. A. Zang, *Spectral Methods in Fluid Dynamics* (Springer, New York, 1987).
[27] D. Funaro, *Polynomial Approximation of Differential Equations* (Springer, New York, 1991).
[28] M. Azaïez, A. Bergeon, and F. Plouraboué, "A new preconditionner for nonseparable elliptic equations," C. R. Mec. **331**, 509 (2003).
[29] R. E. Lynch, J. R. Rice, and D. H. Thomas, "Direct solution for partial difference equations by tensor product methods," Numer. Math. **6**, 185 (1964).
[30] G. E. Karniadakis, M. Israeli, and S. A. Orszag, "High-order splitting method for the incompressible Navier–Stokes," J. Comput. Phys. **97**, 414 (1991).
[31] A. T. Patera, "A spectral element method for fluid dynamics: Laminar flow in a channel expansion," J. Comput. Phys. **54**, 468 (1984).
[32] M. Quintard and S. Whitaker, "Ecoulement monophasique en milieu poreux: effet des heterogeneites locales," J. Mec. Theor. Appl. **6**, 691 (1987).